


## First-principles investigation of magnetocrystalline anisotropy oscillations in $\text{Co}_2\text{FeAl}/\text{Ta}$ heterostructures

Junfeng Qiao,<sup>1,2</sup> Shouzhong Peng,<sup>1,2</sup> Youguang Zhang,<sup>1,2</sup> Hongxin Yang,<sup>3</sup> and Weisheng Zhao<sup>1,2,\*</sup>

<sup>1</sup>Fert Beijing Institute, BDBC, Beihang University, Beijing 100191, China

<sup>2</sup>School of Electronic and Information Engineering, Beihang University, Beijing 100191, China

<sup>3</sup>Key Laboratory of Magnetic Materials and Devices, Ningbo Institute of Materials Technology and Engineering, Chinese Academy of Sciences, Ningbo 315201, China

 (Received 5 December 2017; revised manuscript received 20 January 2018; published 20 February 2018)

We report first-principles investigations of magnetocrystalline anisotropy energy (MCAE) oscillations as a function of capping layer thickness in Heusler alloy  $\text{Co}_2\text{FeAl}/\text{Ta}$  heterostructures. A substantial oscillation is observed in the FeAl-interface structure. According to  $k$ -space and band-decomposed charge-density analyses, this oscillation is mainly attributed to the Fermi-energy-vicinal quantum well states (QWSs) which are confined between the  $\text{Co}_2\text{FeAl}/\text{Ta}$  interface and Ta/vacuum surface. The smaller oscillation magnitude in the Co-interface structure can be explained by the smooth potential transition at the interface. These findings clarify that MCAE in  $\text{Co}_2\text{FeAl}/\text{Ta}$  is not a local property of the interface and that the quantum well effect plays a dominant role in MCAE oscillations of the heterostructures. This work presents the possibility of tuning MCAE by QWSs in capping layers and paves the way for artificially controlling magnetic anisotropy energy in magnetic tunnel junctions.

DOI: [10.1103/PhysRevB.97.054420](https://doi.org/10.1103/PhysRevB.97.054420)

### I. INTRODUCTION

With the increasing demand for high-speed and low-power-consumption storage devices, intensive research has been undertaken on spin-transfer-torque magnetic random access memory (STT-MRAM). The core structure of MRAM is a magnetic tunnel junction (MTJ) [1], which is composed of an insulating barrier sandwiched between two ferromagnetic (FM) electrodes. The relative orientation of the two FM electrodes represents two states and can be utilized to store 1 bit of information. To realize high storage density, the manufacturing process is scaling down to the nanometer regime. However, the increasing process variations in the fabrication pose serious challenges to fundamental physics [2], especially magnetocrystalline anisotropy energy (MCAE), which is critical for the thermal stability of the relative magnetization orientation of the two FM electrodes. Previous work reported that to achieve a retention time of 10 yr, an interfacial perpendicular magnetic anisotropy (PMA) of  $4.7 \text{ mJ/m}^2$  is required for device sizes scaling down to 10 nm [3]. However, at present the most widely used FM electrode, CoFeB, can commonly reach an interfacial PMA of  $1.3 \text{ mJ/m}^2$  when interfaced with a MgO tunneling barrier [1,4–6]. At the same time tunneling magnetoresistance (TMR) can reach a value of 120% in CoFeB/MgO/CoFeB MTJ [1], which needs to be improved as well.

To further promote the development of STT-MRAM, other FM materials are under investigation. Heusler alloys are a big family of ternary intermetallic compounds with nearly 1500 members [7]. According to their chemical composition, Heusler alloys can be separated into two classes, full Heusler

with the chemical composition  $X_2YZ$  ( $L2_1$  structure) and half Heusler  $XYZ$  ( $C1_b$  structure), in which  $X$  and  $Y$  are transition metals and  $Z$  is the main group element [8]. By virtue of the broad choices of elements and stoichiometry, many Heusler compounds exhibit interesting properties, such as half metallicity [9], various Hall effects [10–12], thermoelectric effects [13], topological effects [12], superconductivity [14], etc. Among Heusler alloys,  $\text{Co}_2\text{FeAl}$  (CFA) has attracted a lot of attention due to its high spin polarization and low magnetic damping constant [15,16]. The TMR ratio can reach up to 700% at 10 K and 330% at room temperature (RT) in a  $\text{Co}_2\text{FeAl}/\text{MgO}/\text{CoFe}$  MTJ [17]. The magnetic damping constant  $\alpha$  can reach as low as 0.001 [18], which is beneficial for reducing the STT switching current. Another merit of CFA is its fine lattice matching with MgO. As a result, epitaxial growth of CFA(001)[110] || MgO(001)[100] can be achieved in experiment [19]. All these advantages make CFA a promising candidate for a MTJ electrode material. Regarding the magnetic anisotropy energy (MAE) of CFA, experimental and theoretical results confirmed that the  $\text{Co}_2\text{FeAl}/\text{MgO}$  interface can reach around  $1 \text{ mJ/m}^2$  [20–22]. However, as discussed above, MAE needs to be optimized further. In addition, it is crucial to find out effective ways to artificially control MAE.

Recently, experimental and theoretical results showed that heavy metals (HMs) can induce large variations in physical properties, including MAE, when interfaced with FM materials [23–30]. In practical MTJs, a buffer layer at the bottom and a capping layer on the top are necessary to improve and protect the FM/MgO/FM core structure. Consequently, the choice of capping layer provides us a unique way to control the MAE of the whole structure. On the other hand, when the thickness of these multilayers reaches down to atomic scale, quantum-mechanical (QM) effects start to dominate.

\*weisheng.zhao@buaa.edu.cn

One of the most well-known QM effects is the quantum well (QW), in which the wave functions of the quantum particle are confined by potential barriers and the energy levels are quantized. In spintronics, the milestone effect, giant magnetoresistance (GMR), and its closely related phenomenon, interlayer exchange coupling (IEC), are deeply related to QWs. These effects have been successfully explained by quantum interferences due to reflections at the spacer boundaries [31]. In terms of the influence of quantum well states (QWSs) on MAE, early theoretical works, using tight-binding formalism and a perturbation treatment to spin-orbit coupling (SOC), reported the oscillation of MAE with respect to Pd layer thickness in the Co/Pd system [32]. However, other work which supports interfacial MAE in the Pd/Co/Pd(111) structure also exists [33]. Other than the HM Pd, MAE oscillations with respect to both Co and Cu were found in the Co/Cu system [34]. Since the IEC effects are prominent in these structures [35,36], the formation of QWSs is well confirmed. Indeed, 10 yr later, MAE oscillations were observed in Cu(001)/Co and Ag(001)/Fe [37] and Fe/Cu and Co/Cu structures [38], and the origin of these oscillations was attributed to QWSs. Also, QWS-induced oscillatory IEC was found in the Co/MgO/Co PMA MTJ [39]. Recent first-principles studies have correlated QWSs with MCAE in Ag/Fe and IEC in Fe/Ag/Fe structures [40,41]. These works indicate that the influence of QWS on magnetic properties, specifically MAE, may become salient in some structures.

In this paper, we report *ab initio* calculations of MCAE in CFA/Ta structures and observe MCAE oscillations associated with the Ta layer thickness. These oscillations are further proved to be induced by both majority-spin and minority-spin QWSs confined in Ta layers. The origin of the significant MCAE oscillation is attributed to the repeated traversing of QWSs across Fermi energy and the large SOC of Ta. In all, QWSs that formed in the capping layer provide us a unique method to tune MAE in the MTJ structure.

## II. METHODS

Calculations were performed using the Vienna Ab initio Simulation Package (VASP) based on projector augmented-wave method and a plane-wave basis set [42]. The exchange and correlation terms were described using the generalized gradient approximation in the scheme of the Perdew-Burke-Ernzerhof parameterization [43]. We used a kinetic-energy cutoff of 520 eV and a  $\Gamma$ -centered Monkhorst-Pack  $k$ -point mesh of  $25 \times 25 \times 1$ . The convergence of MCAE relative to the  $k$  point has been checked carefully; the variation of MCAE is about 0.05 meV when changing the  $k$ -point mesh from  $20 \times 20 \times 1$  to  $25 \times 25 \times 1$ , which is at least a magnitude smaller than the oscillation amplitude of MCAE. The energy convergence criteria of all the calculations were set as  $1.0 \times 10^{-7}$  eV, and all the structures were relaxed until the force acting on each atom was less than 0.01 eV/Å. All the structures have at least 15Å vacuum spaces to eliminate interactions between periodic images.

Bulk CFA has a cubic  $L2_1$  crystal structure. After fully relaxing the bulk structure in volume and shape, the lattice constant is found to be  $a_{\text{bulk}} = 5.70$  Å, which closely matches

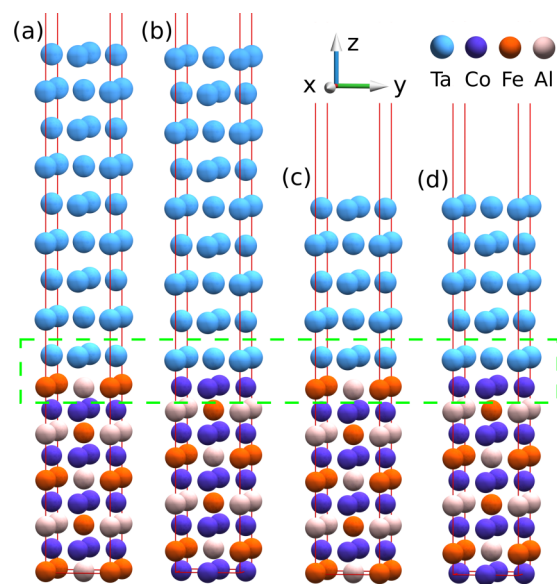


FIG. 1. Crystal structure of (a) FeAl-CFA/Ta[9], (b) Co-CFA/Ta[9], (c) FeAl-CFA/Ta[5], and (d) Co-CFA/Ta[5]. Only four structures are shown as illustrations. In other structures, only the number of Ta MLs is varied, ranging from 1 to 12. The dashed green rectangle highlights the area of the interfaces.

the experimental value of 5.73 Å [44]. For the CFA/Ta heterostructure, an in-plane lattice constant of  $a = a_{\text{bulk}}/\sqrt{2} = 4.03$  Å is adopted for the unit cell, which is rotated by 45° from the conventional cell of bulk CFA. For all the CFA/Ta structures, 9 monolayers (MLs) of CFA are used, and 1 to 12 MLs of Ta layers are put on top of CFA, as shown in Fig. 1. We use CFA/Ta[ $n$ ] to label structures of different Ta MLs, where  $n$  is the number of Ta MLs, ranging from 1 to 12. As for the interface between CFA and Ta, two kinds of configurations exist, and both of them have been investigated. FeAl-CFA/Ta is used as the label when the FeAl layer of CFA directly makes contact with Ta, while Co-CFA/Ta is used when the Co layer of CFA makes contact with Ta.

To calculate MCAE, two-step procedures were adopted. First, charge density was acquired self-consistently without taking into account SOC. Second, reading the self-consistent charge density, two non-self-consistent calculations were performed including SOC, with magnetization pointing towards the [100] direction and the [001] direction. Finally, MCAE was calculated by  $\text{MCAE} = E^{[100]} - E^{[001]}$ ; positive MCAE stands for PMA, while negative MCAE stands for in-plane magnetic anisotropy.

To get a deeper understanding of the origin of the oscillation, MCAE is decomposed into  $k$  space. According to the force theorem [45–47], the main contribution of MCAE originates from the difference in eigenvalues between two magnetization directions. Indeed, we found that the ion Ewald summation energy, Hartree energy, exchange-correlation energy, and external potential energy are exactly the same between the two magnetization directions; the difference in total energy comes only from the difference in eigenvalue summation, which testifies to the feasibility of  $k$ -space decomposition of MCAE.

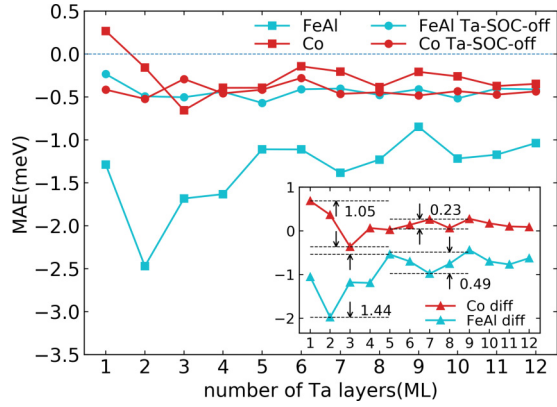


FIG. 2. MCAE oscillation with respect to the Ta ML number. Cyan shows the FeAl-interface structure, and red shows the Co-interface structure. Circles indicate the MCAE calculation with the SOC of Ta switched off while the SOC of CFA is still included; squares show the normal MCAE calculation. Lines in the inset are defined by Eq. (2). The numbers in the inset mark the oscillation magnitude of the first period and the second period.

Specifically, this can be expressed as

$$\text{MCAE}(\mathbf{k}) = \sum_i n_{i,\mathbf{k}}^{[100]} \epsilon_{i,\mathbf{k}}^{[100]} - \sum_{i'} n_{i',\mathbf{k}}^{[001]} \epsilon_{i',\mathbf{k}}^{[001]}, \quad (1)$$

where  $\mathbf{k}$  is the  $k$ -point index,  $i, i'$  are the band indexes of the magnetization direction along [100] and [001], respectively,  $n_{i,\mathbf{k}}$  is the occupation number of this band, and  $\epsilon_{i,\mathbf{k}}$  is the energy of band  $i$  at  $k$  point  $\mathbf{k}$ .

### III. RESULTS AND DISCUSSION

#### A. MCAE oscillation

Unlike the FM/oxide structure where the MCAE can be accounted the local hybridization of the interfacial Fe 3d orbital and the interfacial O 2p orbital [6], the MCAE of CFA/Ta structure varies strongly when the Ta thickness changes. In this circumstance, MCAE cannot be treated as a local property of the interface. We observe a strong oscillation of MCAE in the FeAl-CFA/Ta structure relative to the thickness of the capping layer Ta, as shown in Fig. 2. The oscillation period is approximately 4 MLs, and the oscillation amplitude decreases as the number of Ta MLs increases. This is due to the fact that the confinement effect of QWs will become less prominent when the width of the QWs increases and the bulk states of Ta will account for a larger proportion in all the electron states. Interestingly, the oscillation is smaller in the Co-CFA/Ta structure; the reason for this phenomenon will be discussed later.

To comprehend the origin of the oscillations, we manually tweak the strength of SOC in the structures. Since MCAE comes only from SOC, switching off the SOC of Ta will totally screen out the contribution of Ta to the MCAE of the whole system. For the FeAl-CFA/Ta structure, by suppressing the SOC of Ta while keeping the SOC of CFA, the oscillation of the MCAE relative to the Ta layer thickness disappears (see cyan lines in Fig. 2). For the Co-CFA/Ta structure, a smaller oscillation exists, and the tweaking of the SOC of Ta has little

influence on the MCAE (see red lines in Fig. 2). These strongly indicate that the electron states in Ta play the determinant role in the MCAE oscillations of CFA/Ta structures.

Further analysis can be carried out by defining the MCAE difference

$$\text{MCAE}^{\text{diff}}(n) = \text{MCAE}(n) - \text{MCAE}^{\text{Ta-off}}(n), \quad (2)$$

where  $n$  is the number of Ta MLs and  $\text{MCAE}^{\text{Ta-off}}(n)$  is the result calculated with the SOC of Ta switched off. The  $\text{MCAE}^{\text{diff}}(n)$  will contain only the MCAE contribution originating from Ta layers, as plotted in the inset of Fig. 2. Note three major differences can be discerned. First, the oscillation magnitude of Co-CFA/Ta vanishes much faster than that of FeAl-CFA/Ta. Second, we can define an oscillation period of 4 MLs in FeAl-CFA/Ta, but it is harder to clearly define an oscillation period for Co-CFA/Ta. Third, in Co-CFA/Ta, the mean value of  $\text{MCAE}^{\text{diff}}(n)$  is essentially zero, while the mean value of  $\text{MCAE}^{\text{diff}}(n)$  of FeAl-CFA/Ta largely deviates from zero. The oscillation of physical properties relative to film thickness is a hallmark of QWSs, and these three remarkable differences suggest that for FeAl-CFA/Ta, the electron states in Ta layers may form QWSs and explain the MCAE oscillation. However, for Co-CFA/Ta, since the MCAE oscillation is less prominent, there is less probability to correlate the MCAE oscillation with QWSs in Ta layers. The subsequent section will concentrate on the analysis of MCAE with special electron states and evidence of the existence of QWSs in the FeAl-CFA/Ta structure. The same analytic procedures are also applied to Co-CFA/Ta in the Supplemental Material [48].

#### B. Critical $k$ points and band structure

Employing the  $k$ -space-resolved method, we dissect MCAE into the two-dimensional Brillouin zone (2D-BZ) for FeAl-CFA/Ta[ $n$ ]. Comparing  $k$ -resolved graphs for structures with different Ta layer thicknesses, two critical  $k$  points, which provide large contributions to MCAE, can be selected, i.e.,  $k$  points at  $[k_x, k_y] = [-0.48, -0.2]$  and  $[k_x, k_y] = [0.48, -0.2]$ , as shown in Fig. 3 (since the number of  $k$  points is set as  $25 \times 25 \times 1$ ,  $k_x$  and  $k_y$  are in the range of  $-0.48$  to  $0.48$ ). The SOC breaks the symmetry of the 2D-BZ; contributions to the total MCAE slightly differ from each other between these two  $k$  points. In fact, when considering the symmetry of the crystal structure, these two  $k$  points are identical and locate at the center of the  $M$  point and  $X$  point of the 2D-BZ, and they will be called critical  $k$  points in the following.

According to second-order perturbation theory, the perturbation of SOC to one-electron energies can be written as

$$\delta\epsilon_i = \sum_{i' \neq i} \frac{|(i'|H_{\text{SOC}}|i)|^2}{\epsilon_i - \epsilon_{i'}}, \quad (3)$$

$$E_{\text{corr}}^{\text{axis}} = \sum_i n_i \delta\epsilon_i = \frac{1}{2} \sum_i \sum_{i' \neq i} \frac{n_i - n_{i'}}{\epsilon_i - \epsilon_{i'}} |(i'|H_{\text{SOC}}^{\text{axis}}|i)|^2,$$

$$\text{axis} = [100], [001], \quad (4)$$

where  $i, i'$  are the quantum numbers of one-electron states,  $\epsilon_i$  is the one-electron energy,  $H_{\text{SOC}}$  is the Hamiltonian of the SOC, axis is the magnetization direction, and  $E_{\text{corr}}^{\text{axis}}$  is the energy correction to the unperturbed state caused by SOC.

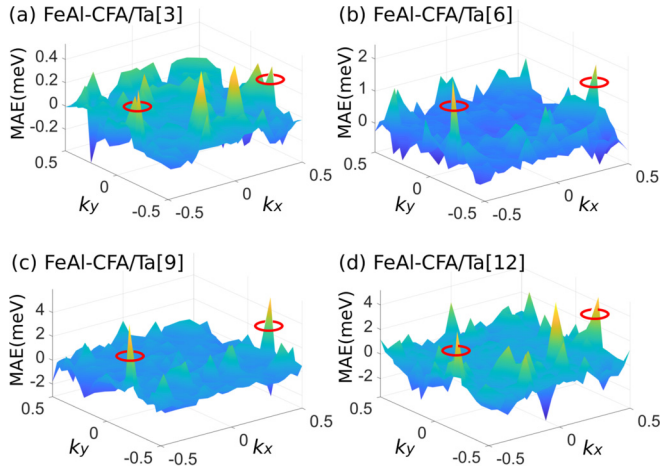


FIG. 3. The  $k$ -resolved graphs of MCAE in the 2D-BZ for (a) FeAl-CFA/Ta[3], (b) FeAl-CFA/Ta[6], (c) FeAl-CFA/Ta[9], and (d) FeAl-CFA/Ta[12]. Critical  $k$  points at  $[k_x, k_y] = [-0.48, -0.2]$  and  $[k_x, k_y] = [0.48, -0.2]$  are labeled by red circles, which provide the dominant contributions to total MCAE.

This expression indicates that only electron states near Fermi energy have maximal impact on MCAE. To extract more information about states contributing the most to the

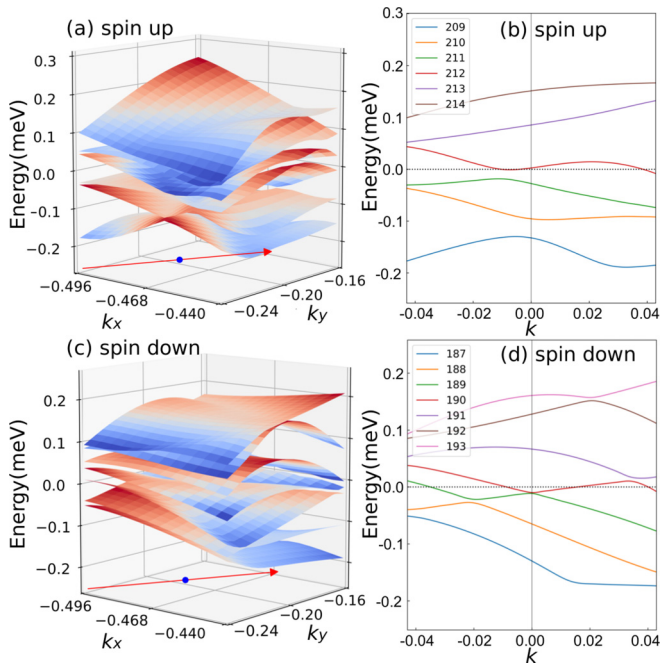


FIG. 4. (a) Three-dimensional spin-up band structure of FeAl-CFA/Ta[9] in a rectangular region around the critical  $k$  point  $[k_x, k_y] = [-0.48, -0.2]$ , which is marked as a blue dot in the horizontal plane. The color represents the relative magnitude of energy in the same band, with larger values in red and smaller values in blue. (b) Spin-up band structure along the line  $k_y = 2.57k_x + 1.03$  as an example, i.e., the red line with an arrow in (a). (c) Three-dimensional spin-down band structure of FeAl-CFA/Ta[9] in the rectangular region. (d) Spin-down band structure along the line  $k_y = 2.57k_x + 1.03$ . The numbers in the legends of (b) and (d) are the band indexes. These bands are vicinal to Fermi energy and have large contributions to the total MCAE.

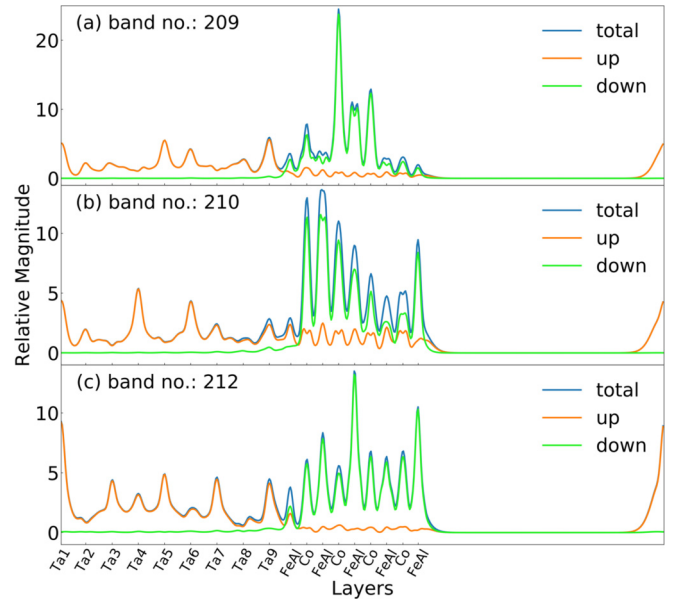


FIG. 5. Charge densities of energy bands at indexes (a) 209, (b) 210, and (c) 212. Green shows the spin-down electron, orange illustrates the spin-up electron, and blue indicates the total charge density. The horizontal axes of these figures correspond to the  $z$  axis of the crystal structure. Note the energies corresponding to the spin-up electrons of these bands are vicinal to Fermi energy, while energies corresponding to the spin-down electrons are higher than Fermi energy due to exchange splitting. The spin-up electrons are mostly confined in Ta layers.

MCAE oscillation, we systematically examine spin-resolved band structures along different directions at this  $k$  point. As an example, we draw the band structure along the line  $k_y = 2.57k_x + 1.03$ , with the band index ranging from 209 to 214, as shown in Fig. 4(b) for spin-up electrons, and from band 187 to 193 for spin-down electrons, as shown in Fig. 4(d). We find that the spin-up band with an index of 212 and a spin-down band with an index of 190 traverse Fermi energy along most of the directions in the 2D-BZ. As a reminder, this particular number has no physical meaning and only labels the order of Kohn-Sham eigenvalues in the calculation result. Note that due to exchange splitting, the energy of the spin-down band is higher than that of the corresponding spin-up band, which has a band index identical to that of the spin-down band, so the Fermi-energy-vicinal bands are different for spin-up and spin-down electrons and should be considered separately.

For Co-CFA/Ta, we find that different from FeAl-CFA/Ta, the rapid variations in the 2D-BZ make the ascription of MCAE oscillation to a specific electron state a bit more difficult. We can still select critical  $k$  points, but the magnitude of the peak does not have a sharp contrast with other  $k$  points, as shown in Fig. S1 in the Supplemental Material [48].

### C. Characterization of QWSs

To explore the nature of these specific electron states, the band-decomposed charge densities of these Fermi-energy-vicinal states are plotted, and we conclude that these are

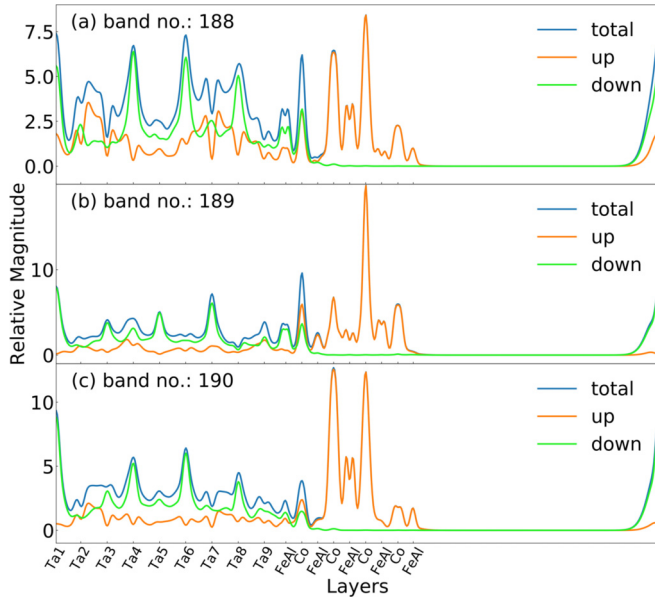


FIG. 6. Charge densities of energy bands at indexes (a) 188, (b) 189, and (c) 190. Note the energies corresponding to the spin-down electrons of these bands are vicinal to the Fermi energy. The spin-down electrons of these bands are confined in Ta layers, while spin-up electrons couple to the states in CFA to some extent.

the quantum well states confined between the FeAl-CFA/Ta interface and the Ta/vacuum surface, as shown in Fig. 5 for spin-up electrons and Fig. 6 for spin-down electrons. Note spin-up electrons of bands from 209 to 212 are Fermi energy vicinal, while for spin-down Fermi-energy-vicinal states, their band indexes are from 188 to 190. The Fermi-energy-vicinal states of both majority spin and minority spin, i.e., spin-up and spin-down electrons, are mostly confined in Ta layers, as indicated by the orange lines in Fig. 5 and green lines in Fig. 6. With increasing band index, more wave crests, which are the characteristic feature of QWSs, are formed. The energies of QWSs depend on the width of the well, namely, the thickness of the Ta layer. By increasing or decreasing Ta layer thickness, the QWSs will fall or rise through the Fermi energy, consequently leading to the oscillation of the total MCAE, as suggested by Eq. (4).

For the Co-CFA/Ta structure, the band-decomposed charge densities of Fermi-energy-vicinal states do not perfectly resemble that of an idealized one-dimensional quantum well with infinite potential barriers; the character of the QWSs is less apparent than that of FeAl-CFA/Ta. Band-decomposed charge densities of Co-CFA/Ta[9] are plotted in Figs. S3 and S4 in the Supplemental Material [48].

Before concluding the charge-density analysis, we would like to clarify that both Figs. 5 and 6 are band decomposed, while the total charge density should be the sum of all the occupied bands. So the crests in the band-decomposed charge densities do not imply a large antiferromagnetic coupling between Ta layers and CFA. The magnetic moments of all the atoms are plotted in Fig. S5 for FeAl-CFA/Ta[9] and Fig. S6 for Co-CFA/Ta[9] for interested readers [48].

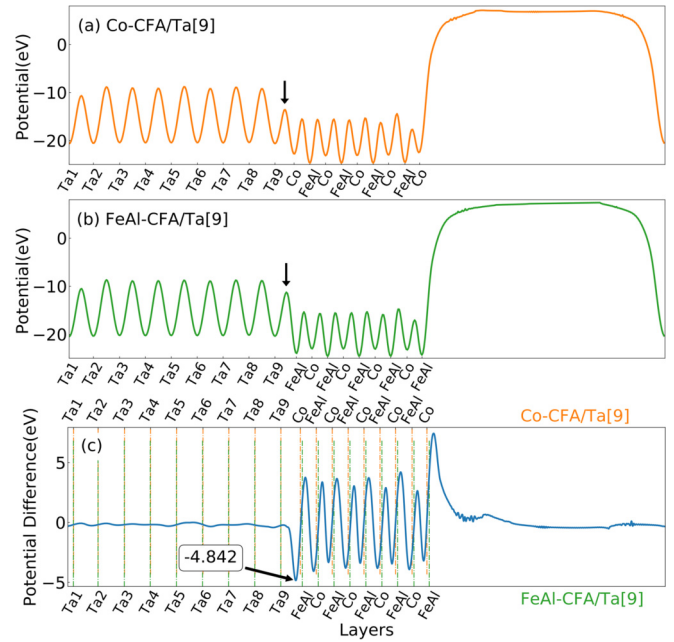


FIG. 7. Potentials along the crystallographic  $z$  direction of (a) Co-CFA/Ta[9] and (b) FeAl-CFA/Ta[9]. (c) Potential difference between the Co-CFA/Ta[9] structure and the FeAl-CFA/Ta[9] structure, where the upper horizontal axis is for Co-CFA/Ta[9] and the lower horizontal axis is for FeAl-CFA/Ta[9]. The black arrows in (a) and (b) mark the location of the interfaces. The dashed orange and green lines represent the  $z$  coordinates of each layer in Co-CFA/Ta[9] and FeAl-CFA/Ta[9], respectively. A potential difference of 4.842 eV can be found between two structures at the interfaces.

#### D. Interface potential

The phenomenon in which only the FeAl-CFA/Ta structure has a strong MCAE oscillation can be understood by the interface potential difference. The potential drop at the interface determines the magnitude of confinement of electrons. The potential of the FeAl layer differs substantially from that of the Co layer. As shown in Fig. 7, a larger mismatch of the potential between Ta and FeAl-CFA is found, while the mismatch between Ta and Co-CFA is much smoother. Since the construction of the initial structures and the processes of atomic relaxations inevitably lead to a small displacement along the  $z$  axis between two structures of different interfaces and the potential difference strongly relies on the origins of coordinates in two structures, we choose part of the Ta layers for sampling and minimize the square error to accurately align these two structures; that is, the potential difference is calculated as

$$V_{\text{diff}}(z) = V_{\text{Co}}(z) - V_{\text{FeAl}}(z + \delta), \quad (5)$$

where

$$\delta = \arg \min_{\epsilon} \left\{ \int [V_{\text{Co}}^{Ta}(z) - V_{\text{FeAl}}^{Ta}(z + \epsilon)]^2 dz \right\}, \quad (6)$$

where  $z$  is the coordinate along the  $z$  axis,  $\delta$  is the displacement of the FeAl-interface structure that accurately aligns two structures, and  $V_{\text{Co}}$  and  $V_{\text{FeAl}}$  are the potentials of Co-CFA/Ta[9] and FeAl-CFA/Ta[9], respectively.  $V_{\text{Co}}^{Ta}$  and  $V_{\text{FeAl}}^{Ta}$  are the potentials of the Ta layers of Co-CFA/Ta[9] and

FeAl-CFA/Ta[9], respectively.  $V_{\text{diff}}(z)$  is the potential difference plotted in Fig. 7(c).

By carefully aligning the Ta layers of FeAl-interface and Co-interface structures to the same position, little difference is found in the Ta part between the structures. But at the interface, the potential is 4.8 eV higher in FeAl-CFA/Ta than in Co-CFA/Ta [see Fig. 7(c)]. This larger mismatch ultimately makes the confinement effect more prominent in the FeAl-CFA/Ta structure, thus explaining the larger magnitude of the MCAE oscillation. The smoother transition of the potential in Co-CFA/Ta does not strongly confine electrons into Ta layers; consequently, the MCAE oscillation relative to Ta layer thickness vanishes faster in the Co-interface structure.

#### IV. CONCLUSIONS

By means of first-principles calculations, we observed a significant oscillation of MCAE as a function of heavy-metal layer thickness in the CFA/Ta structure with the FeAl interface. The origin of this oscillation can be attributed to electron state confinement in Ta layers. Through  $k$ -space analysis, states with the largest contribution to MCAE can be traced to special  $k$  points located at the center of the  $X$  point and

the  $M$  point in the 2D-BZ. Moreover, it was unveiled that the Fermi-energy-vicinal states contribute the most to total MCAE. The wave crests and troughs appearing in these bands indicate that these are the quantum well states confined in Ta layers. The smaller oscillation magnitude in the Co-interface structure can be explained by the smoother potential transition at the Co/Ta interface, which imposes less confinement on electrons in Ta layers. This work clarifies that due to the QWSs in the capping layer, MCAE in CFA/Ta cannot be accounted a local property of the interface. Other than the commonly used approach of inducing MAE with the FM/MgO interface, we demonstrated that QWSs formed in the capping layer provide a way to artificially control MAE in nanostructures, which could promote the development of STT-MRAM.

#### ACKNOWLEDGMENTS

The authors are thankful for the support from the projects from the National Natural Science Foundation of China (Grants No. 61571023, No. 61501013, and No. 61627813), the Beijing Municipal of Science and Technology (Grant No. D15110300320000), and the International Collaboration Project (Grants No. 2015DFE12880 and No. B16001).

- 
- [1] S. Ikeda, K. Miura, H. Yamamoto, K. Mizunuma, H. D. Gan, M. Endo, S. Kanai, J. Hayakawa, F. Matsukura, and H. Ohno, *Nat. Mater.* **9**, 721 (2010).
  - [2] W. Kang, L. Zhang, J. O. Klein, Y. Zhang, D. Ravelosona, and W. Zhao, *IEEE Trans. Electron Devices* **62**, 1769 (2015).
  - [3] S. Peng, W. Kang, M. Wang, K. Cao, X. Zhao, L. Wang, Y. Zhang, Y. Zhou, K. L. Wang, and W. Zhao, *IEEE Magn. Lett.* **8**, 3105805 (2017).
  - [4] H. X. Yang, M. Chshiev, B. Dieny, J. H. Lee, A. Manchon, and K. H. Shin, *Phys. Rev. B* **84**, 054401 (2011).
  - [5] A. Hallal, H. X. Yang, B. Dieny, and M. Chshiev, *Phys. Rev. B* **88**, 184423 (2013).
  - [6] B. Dieny and M. Chshiev, *Rev. Mod. Phys.* **89**, 025008 (2017).
  - [7] T. Graf, C. Felser, and S. S. Parkin, *Prog. Solid State Chem.* **39**, 1 (2011).
  - [8] S. Trudel, O. Gaier, J. Hamrle, and B. Hillebrands, *J. Phys. D* **43**, 193001 (2010).
  - [9] I. Galanakis, P. H. Dederichs, and N. Papanikolaou, *Phys. Rev. B* **66**, 174429 (2002).
  - [10] A. Husmann and L. J. Singh, *Phys. Rev. B* **73**, 172417 (2006).
  - [11] I. Dubenko, A. K. Pathak, S. Stadler, N. Ali, Y. Kovarskii, V. N. Prudnikov, N. S. Perov, and A. B. Granovsky, *Phys. Rev. B* **80**, 092408 (2009).
  - [12] S. Chadov, X. Qi, J. Kübler, G. H. Fecher, C. Felser, and S. C. Zhang, *Nat. Mater.* **9**, 541 (2010).
  - [13] Y. K. Kuo, K. M. Sivakumar, H. C. Chen, J. H. Su, and C. S. Lue, *Phys. Rev. B* **72**, 054116 (2005).
  - [14] D. Sprungmann, K. Westerholt, H. Zabel, M. Weides, and H. Kohlstedt, *Phys. Rev. B* **82**, 060505 (2010).
  - [15] Z. Bai, L. Shen, G. Han, and Y. P. Feng, *SPIN* **2**, 1230006 (2012).
  - [16] H. Sukegawa, Z. C. Wen, S. Kasai, K. Inomata, and S. Mitani, *SPIN* **4**, 1440023 (2014).
  - [17] W. Wang, H. Sukegawa, R. Shan, S. Mitani, and K. Inomata, *Appl. Phys. Lett.* **95**, 182502 (2009).
  - [18] S. Mizukami, D. Watanabe, M. Oogane, Y. Ando, Y. Miura, M. Shirai, and T. Miyazaki, *J. Appl. Phys.* **105**, 07D306 (2009).
  - [19] M. S. Gabor, T. Petrisor, C. Tiusan, M. Hehn, and T. Petrisor, *Phys. Rev. B* **84**, 134413 (2011).
  - [20] Z. Wen, H. Sukegawa, S. Mitani, and K. Inomata, *Appl. Phys. Lett.* **98**, 242507 (2011).
  - [21] Z. Wen, H. Sukegawa, T. Furubayashi, J. Koo, K. Inomata, S. Mitani, J. P. Hadorn, T. Ohkubo, and K. Hono, *Adv. Mater.* **26**, 6483 (2014).
  - [22] R. Vadapoo, A. Hallal, H. Yang, and M. Chshiev, *Phys. Rev. B* **94**, 104418 (2016).
  - [23] S. Ouazi, S. Vlaic, S. Rusponi, G. Moulas, P. Bulushek, K. Halleux, S. Bornemann, S. Mankovsky, J. Minár, J. B. Staunton, H. Ebert, and H. Brune, *Nat. Commun.* **3**, 1313 (2012).
  - [24] C. Andersson, B. Sanyal, O. Eriksson, L. Nordström, O. Karis, D. Arvanitis, T. Konishi, E. Holub-Krappe, and J. H. Dunn, *Phys. Rev. Lett.* **99**, 177207 (2007).
  - [25] C.-F. Pai, M.-H. Nguyen, C. Belvin, L. H. Vilela-Leão, D. C. Ralph, and R. A. Buhrman, *Appl. Phys. Lett.* **104**, 082407 (2014).
  - [26] J. Zhou, W. Zhao, Y. Wang, S. Peng, J. Qiao, L. Su, L. Zeng, N. Lei, L. Liu, Y. Zhang, and A. Bournel, *Appl. Phys. Lett.* **109**, 242403 (2016).
  - [27] B. Zhang, A. Cao, J. Qiao, M. Tang, K. Cao, X. Zhao, S. Eimer, Z. Si, N. Lei, Z. Wang, X. Lin, Z. Zhang, M. Wu, and W. Zhao, *Appl. Phys. Lett.* **110**, 012405 (2017).
  - [28] P. Gambardella, S. Rusponi, M. Veronese, S. S. Dhesi, C. Grazioli, A. Dallmeyer, I. Cabria, R. Zeller, P. H. Dederichs, K. Kern, C. Carbone, and H. Brune, *Science* **300**, 1130 (2003).

- [29] T. Balashov, T. Schuh, A. F. Takács, A. Ernst, S. Ostanin, J. Henk, I. Mertig, P. Bruno, T. Miyamachi, S. Suga, and W. Wulfhekel, *Phys. Rev. Lett.* **102**, 257203 (2009).
- [30] S. Peng, W. Zhao, J. Qiao, L. Su, J. Zhou, H. Yang, Q. Zhang, Y. Zhang, C. Grezes, P. K. Amiri, and K. L. Wang, *Appl. Phys. Lett.* **110**, 072403 (2017).
- [31] P. Bruno and C. Chappert, *Phys. Rev. Lett.* **67**, 1602 (1991).
- [32] M. Cinal and D. M. Edwards, *Phys. Rev. B* **55**, 3636 (1997).
- [33] J. Dorantes-Dávila, H. Dreyssé, and G. M. Pastor, *Phys. Rev. Lett.* **91**, 197206 (2003).
- [34] L. Szunyogh, B. Újfalussy, C. Blaas, U. Pustogowa, C. Sommers, and P. Weinberger, *Phys. Rev. B* **56**, 14036 (1997).
- [35] S. S. P. Parkin, *Phys. Rev. Lett.* **67**, 3598 (1991).
- [36] Z. Celinski and B. Heinrich, *J. Magn. Magn. Mater.* **99**, L25 (1991).
- [37] M. Przybylski, M. Dąbrowski, U. Bauer, M. Cinal, and J. Kirschner, *J. Appl. Phys.* **111**, 07C102 (2012).
- [38] S. Manna, P. L. Gastelois, M. Dąbrowski, P. Kuświk, M. Cinal, M. Przybylski, and J. Kirschner, *Phys. Rev. B* **87**, 134401 (2013).
- [39] L. E. Nistor, B. Rodmacq, S. Auffret, A. Schuhl, M. Chshiev, and B. Dieny, *Phys. Rev. B* **81**, 220407 (2010).
- [40] C.-H. Chang, K.-P. Dou, Y.-C. Chen, T.-M. Hong, and C.-C. Kaun, *Sci. Rep.* **5**, 16844 (2015).
- [41] C.-H. Chang, K.-P. Dou, G.-Y. Guo, and C.-C. Kaun, *NPG Asia Mater.* **9**, e424 (2017).
- [42] G. Kresse and J. Furthmüller, *Phys. Rev. B* **54**, 11169 (1996).
- [43] G. Kresse and D. Joubert, *Phys. Rev. B* **59**, 1758 (1999).
- [44] G. Ortiz, M. S. Gabor, J. T. Petrisor, F. Boust, F. Issac, C. Tiusan, M. Hehn, and J. F. Bobo, *J. Appl. Phys.* **109**, 07D324 (2011).
- [45] D.-s. Wang, R. Wu, and A. J. Freeman, *Phys. Rev. B* **47**, 14932 (1993).
- [46] G. H. O. Daalderop, P. J. Kelly, and M. F. H. Schuurmans, *Phys. Rev. B* **50**, 9989 (1994).
- [47] X. Wang, D. S. Wang, R. Wu, and A. Freeman, *J. Magn. Magn. Mater.* **159**, 337 (1996).
- [48] See Supplemental Material at <http://link.aps.org/supplemental/10.1103/PhysRevB.97.054420> for the analysis of Co-CFA/Ta and magnetic moments.